Technology in Cancer Research & Treatment
ISSN 1533-0346
Volume 1, Number 1, February (2002)

Noninvasive Native Fluorescence Imaging of Head and Neck Tumors

www.tcrt.org

A. Katz, Ph.D. [1]
Howard E. Savage, Ph.D. [2]
Stimson P. Schantz, M.D. [3]
Steven A. McCormick, M.D. [2]
and R. R. Alfano, Ph.D.[1]*

[1]New York State Center for Advanced Technology in Ultrafast Photonics
Institute for Ultrafast Spectroscopy and Lasers
Convent Avenue & 137 St.
The City College of New York
New York, NY 10031, USA

[2]Department of Pathology
New York Eye and Ear Infirmary
310 East 14th Street
New York, NY 10003, USA

[3]Department of Otolaryngology
New York Eye and Ear Infirmary
310 East 14th Street
New York, NY 10003, USA

Fluorescence images were acquired from *ex vivo* head and neck tumor specimens. The excitation and emission wavelength combinations were selected to image emission from native tissue fluorophores (collagen, tryptophan, elastin and nicotinamide adenine dinucleotide). Two dimensional intensity ratio maps were generated from the fluorescence images and compared to histology images. The ratio maps accurately distinguished the regions of tumor from normal tissue in the specimens. Additional features, such as collagen capsules, blood vessels, mucus glands and muscles were evident in the fluorescence images.

Introduction

The use of fluorescence spectroscopy to interrogate the state of a tissue can provide a real-time, noninvasive diagnostic aid to detect precancer and cancer. Native fluorescence was first applied to the detection of cancer in animal, and later in human, *ex vivo* tissues by Alfano *et al* (1,2). This technology was given the name "Optical Biopsy". Over the years, Optical Biopsy was extended to include tissues of many different organs (3). The use of excitation and emission spectroscopy in the ultraviolet (UV) has produced diagnostic accuracies greater than 90% using algorithms based on ratios of emission intensities at key wavelengths (3-5). This improvement in diagnostic accuracy was the direct result of optical interrogation of tissue fluorophores such as tryptophan, nicotinamide adenine dinucleotide (NADH), nucleic acids, elastin and collagen. The wavelengths employed in the ratio algorithms corresponded to the absorption and emission bands of the above mentioned fluorophores. Algorithms based on intensity ratios have some advantages: intensity ratio algorithms are independent of fluctuations in excitation power and collection geometry; ratio algorithms eliminate the need to acquire complete spectra, thereby reducing the data acquisition times – a potentially significant factor in clinical application; and intensity-based ratio algorithms are well suited for application to fluorescence imaging, where images may be acquired at a relatively small number of wavelengths.

Prior studies on *ex vivo* tissues have consistently demonstrated that the ratio of tryptophan emission (λ_{ex} = 300 nm; λ_{em} = 340 nm) to NADH emission (λ_{ex} = 300 nm; λ_{em} = 440 nm) was higher for malignant tissue than for non-malignant tissue (3,4). Glasgold *et al*,(6) using a rat esophagus model, demonstrated that changes in basal cell layer thickness can be observed in both emission (340 nm excitation) and excitation spectra (380 nm emission). In that work, it was shown that the thickening of the basal cell layer resulting from tumor growth, produces a corresponding reduction of collagen emission from the underlying stroma. The changes in the emission spectra were observed in the ratio of the intensity of the 390 nm emission to the 450 nm emission. The changes in the excitation spectra were observed in ratio of emission intensity with 330 nm excitation to the emis-

* Corresponding author:
R.R. Alfano, Ph.D.
E-mail: alfano@scisun.sci.ccny.cuny.edu

sion intensity with 280 nm excitation. That the spectral changes in this study were observable prior to visual indication of tumor demonstrated the potential of fluorescence spectroscopy to detect premalignancy. *Ex vivo* human (7) and animal studies (8) of oral mucosa in the visible spectral region have also identified differences between normal, malignant and premalignant lesions.

In a clinical study, Schantz *et al* investigated the of fluorescence properties of the oral cavity (9-11). In their work, intensity ratios from both emission and excitation spectra were shown to be able to differentiate normal oral mucosa from dysplastic and cancerous mucosa. The results of these studies formed the basis for selection of the excitation and emission wavelengths of the fluorescence imaging system employed in this research.

In the present work, images of fluorescence emission from native fluorophores in *ex vivo* head and neck tumor specimens were acquired at multiple combinations of emission and excitation wavelengths for the purposes of identifying features which may be indicative of malignancy. Fluorescence maps were generated by ratioing fluorescence image intensities. These fluorescence ratio maps enhanced the ability to recognize regions of tumor and other features in tissues. Histopathological analysis was performed on the tissue samples. Location and shape of features observed in the fluorescence images were correlated with structures observed in histopathology.

Materials and Methods

Specimen preparation

Fluorescence images were acquired from freshly resected head and neck tumors. Specimen sizes were in the range of 1 to 2 cm. Prior to acquisition of the fluorescence images, specimens were stored at 4∞C, and except for being kept moist with PBS solution, were not chemically treated. Immediately after image acquisition, specimens were marked to facilitate comparisons between histopathology photomicrographs and the fluorescence images. Specimens were then placed in formalin for subsequent histopathological analysis.

Fluorescence Imaging System

The fluorescence imaging system used to acquire the data presented in this study is a breadboard system developed at The City College of New York by the authors, and named the CD-Map. Excitation light is provided by a broadband xenon lamp and delivered to the specimen by a UV transmitting light pipe. The angle between the light pipe and the collection optics was minimized to provide more uniformity of illumination and to reduce shadows. Excitation wavelength is selected by narrow band optical interference filters with a bandwidth of 10 nm Full Width at Half Maximum (FWHM). The emitted light is collected by UV transmitting lenses and imaged onto the photo cathode of UV sensitive image intensifier. Emission wavelength is selected by optical interference filters with a bandwidth of 10 nm FWHM. The gain of the CD-Map can be adjusted by modifying the voltage on the intensifier or by changes the f-number of the collection lens. The image output of the intensifier is relayed to a video camera and transferred to a Personnel Computer at video rate (30 frames per second). A frame grabber in the host computer digitizes the images at 640 - 480 pixel resolution with an 8 bit Analog-to-Digital converter. Individual frames are stored on the host computer for averaging at a later time. The field of view of the CD-Map is approximately 2 cm. The limiting element in defining spatial resolution of this system is the image intensifier and the spatial resolution is better than 100 µm. A schematic of the CD-Map is shown in Figure 1.

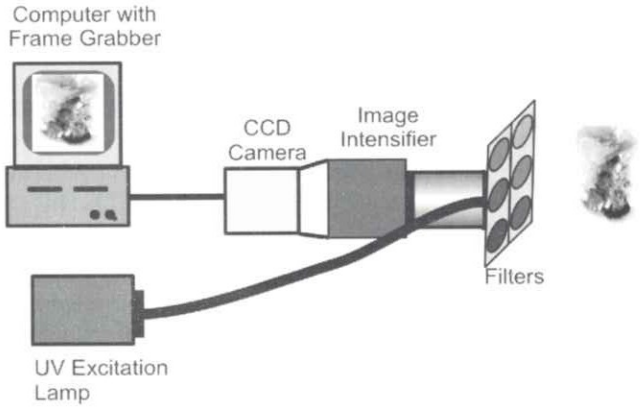

Figure 1: Schematic of breadboard CD-Map.

Image Acquisition

Specimens were imaged with three excitation and three emission wavelengths for a total of six fluorescence images. These wavelength combinations interrogate tryptophan, collagen, NADH and elastin. From these six images, two excitation and two emission ratio maps were generated. To create an emission ratio, the specimen is excited at a wavelength at which both fluorophores of interest absorb, and the emission intensity is measured at two distinct wavelengths, each wavelength being in the emission band of a fluorophore. The ratio map is generated by dividing the two emission intensities, pixel by pixel. To create an excitation ratio, the emission bands of the two fluorophores of interest should have some overlap. First the sample is excited at a wavelength for which only one of the fluorophore absorbs, and the emission intensity is measured. Next, without changing emission wavelength, the specimen is excited at a wavelength for which only the other fluorophore absorbs and

emission intensity is measured again. The ratio map is generated by dividing the two emission images.

The wavelength combinations for the six fluorescence images are: I_1 (λ_{ex} = 300 nm, λ_{em} = 340 nm); I_2 (λ_{ex} = 300 nm, λ_{em} = 380 nm); I_3 (λ_{ex} = 300 nm, λ_{em} = 440 nm); I_4 (λ_{ex} = 340 nm, λ_{em} = 380 nm); I_5 (λ_{ex} = 340 nm, λ_{em} = 440 nm); and I_6 (λ_{ex} = 380 nm, λ_{em} = 440 nm). I_1 and I_2 measures tryptophan emission, I_3 measures NADH emission, I_4 measures collagen emission, and I_5 and I_6 measure NADH and elastin emission. The four ratio maps which were calculated are: (1) $R_1 = I_{340}/I_{440}$, λ_{ex} = 300 nm; (2) $R_2 = I_{380}/I_{440}$, λ_{ex} = 340 nm; (3) $R_3 = I_{300}/I_{340}$, λ_{em} = 380 nm; and (4) $R_4 = I_{340}/I_{380}$, λ_{em} = 440 nm. The fluorescence image and ratio wavelengths are summarized in Table I. For each image, 25 frames were collected and averaged for a total integration time of 750 milliseconds per image. Computer overhead increased the total time to acquire an image by approximately 5 seconds. In a clinical application, the overhead can be eliminated by the use of a faster computer with greater memory and improvements in software efficiency.

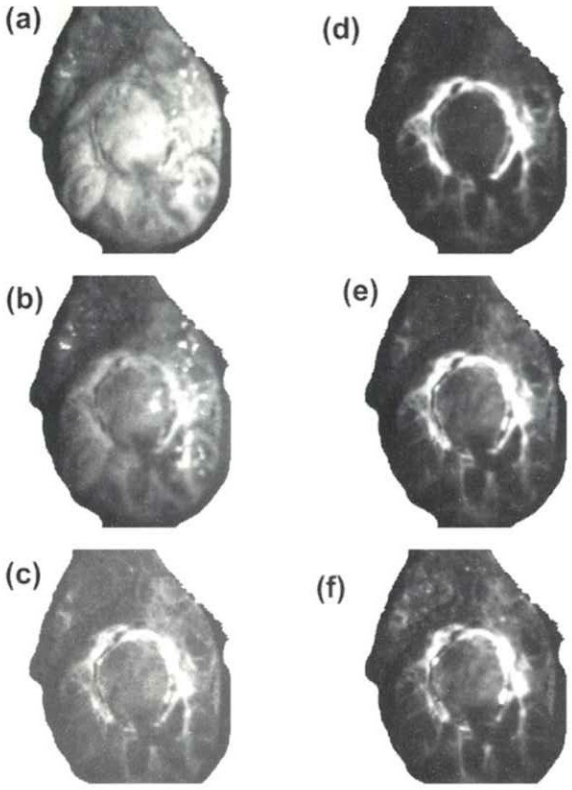

Figure 2: Fluorescence images from thyroid papillary carcinoma inside collagen capsule. Excitation/emission wavelengths are (a) λ_{ex} = 300 nm; λ_{em} = 340 nm; (b) λ_{ex} = 300 nm; λ_{em} = 380 nm; (c)λ_{ex} = 300 nm; λ_{em} = 440 nm; (d) λ_{ex} = 340 nm; λ_{em} = 380 nm; (e) λ_{ex} = 340 nm; λ_{em} = 440 nm; and (f) λ_{ex} = 380 nm; λ_{em} = 440 nm. The tumor is both inside capsule and in the bottom and left sides of the specimen.

Ratio maps were generated by converting the pixel data from 2 byte integer format to floating point values and performing a pixel by pixel division to create a two dimensional map array. This map array was then normalized and converted to 8 bit integer values to utilize the full 8 bit dynamic range of Microsoft Windows(tm) gray level bitmaps. This facilitated display of images on a Personal Computer. Pseudo color was added to the maps by modifying the lookup palettes for the bitmap images.

Ultraviolet exposure risk

Since the Optical Biopsy technology has the highest accuracy when employed in the UV spectral region, the issue of UV exposure should be addressed before this imaging technology is applied *in vivo*. The excitation intensity of the CD-Map at 300 nm is 1 mW/cm^2 at the specimen site. With elimination of computer overhead, the total fluence at 300 nm would be 2.25 mJ/cm^2, this compares to the Minimal Erythema Dosage (MED) of 10 mJ/cm^2 for 300 nm radiation, set by the American College of Governmental and Industrial Hygienists (ACGIH) (12). The human biological response falls over rapidly for wavelengths longer than 310 nm, thus the excitation at 340 and 380 nm offer negligible contribution to the total UV exposure risk. Therefore, the UV exposure fluence from the CD-Map would be within acceptable levels for clinical application.

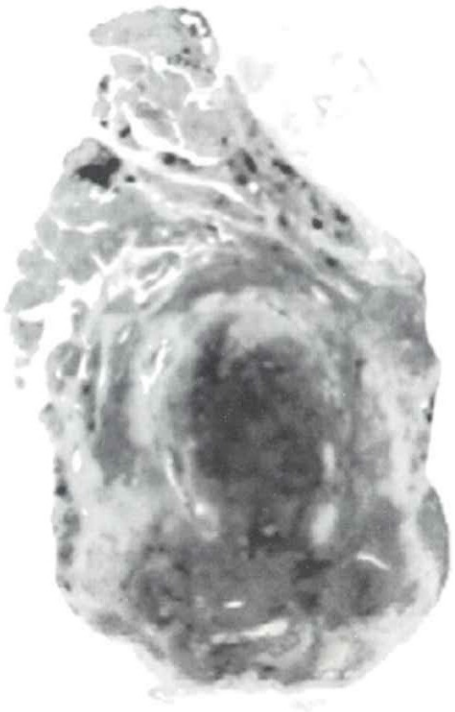

Figure 3: Histology photomicrograph of the thyroid papillary carcinoma.

Results and Discussion

All specimens examined in this research exhibited some similar spectral characteristics in their respective fluorescence images. The tumor regions of the samples consistently demonstrated significantly weaker emission intensity from collagen and NADH. Some of the specimens exhibited relatively lower intensity emission from tryptophan from the normal regions as compared to the tumor regions. Since the tryptophan emission band, which peaks at 340 nm, overlaps the collagen absorption band, the decrease in tryptophan emission intensity is likely a result a tryptophan emission being reabsorbed by collagen. Fluorescence images, ratio maps and corresponding histopathology from three specimens will be presented below.

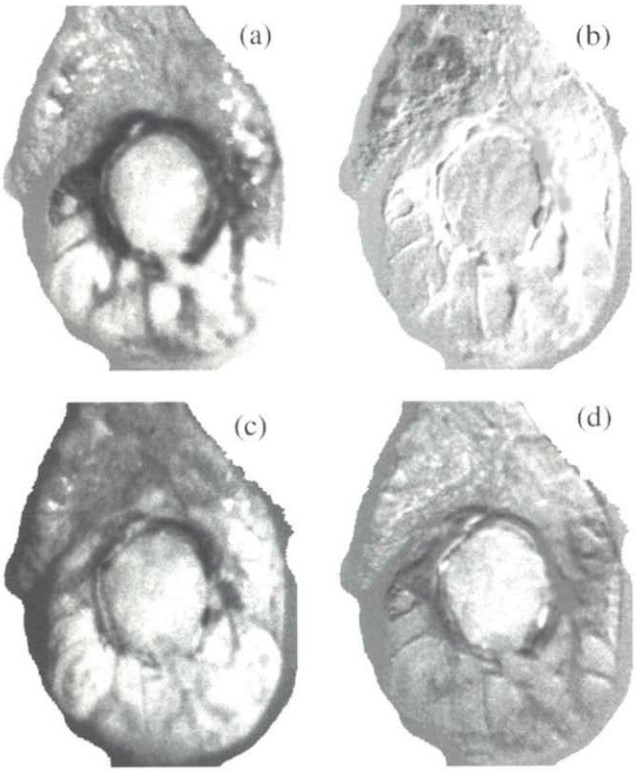

Figure 4: Intensity ratio maps generated from the fluorescence images shown in Figure 3. Ratio wavelengths are: (a) R_1 (I_{340}/I_{440}, λ_{ex} = 300 nm); (b) R_2 (I_{380}/I_{440}, λ_{ex} = 340 nm); (c) R_3 (I_{300}/I_{340}, λ_{em} = 380 nm); and (d) R_4 (I_{340}/I_{380}, λ_{em} = 440 nm).

Thyroid Papillary Carcinoma

The ability of fluorescence imaging to locate and identify tumor regions as well as other structures in tissues is evidenced in the results of the fluorescence images from the thyroid specimen displayed in Figures 2(a)-(f). Located in the middle of this specimen is a papillary carcinoma surrounded by a collagen capsule, typical of this type of invasive carcinoma. The tumor has broken out of the capsule at the bottom, and histological analysis reveals smaller regions of tumor at the bottom and left side of the specimen. Histopathology identified the top section of the specimen as normal tissue. Consider the fluorescence image shown in Fig. 2(a), (λ_{ex} = 300 nm; λ_{em} = 340 nm). The shell of the capsule is identifiable by a less intense ring surrounding the high emission intensity region inside the capsule. Additional, smaller areas of high tryptophan emission are evident at the bottom and to the left of the capsule. The reason that the capsule appears dark in this image is because has high absorption at 340 nm due to the high concentration of collagen and therefore a significant part of the tryptophan emission is being reabsorped. The tumor areas, the excitation light does not reach the underlying stroma and therefore there is no reabsorption of the 340 nm emission by collagen. The normal tissue in the upper half of the image exhibits less tryptophan emission than the areas of tumor. The image shown in

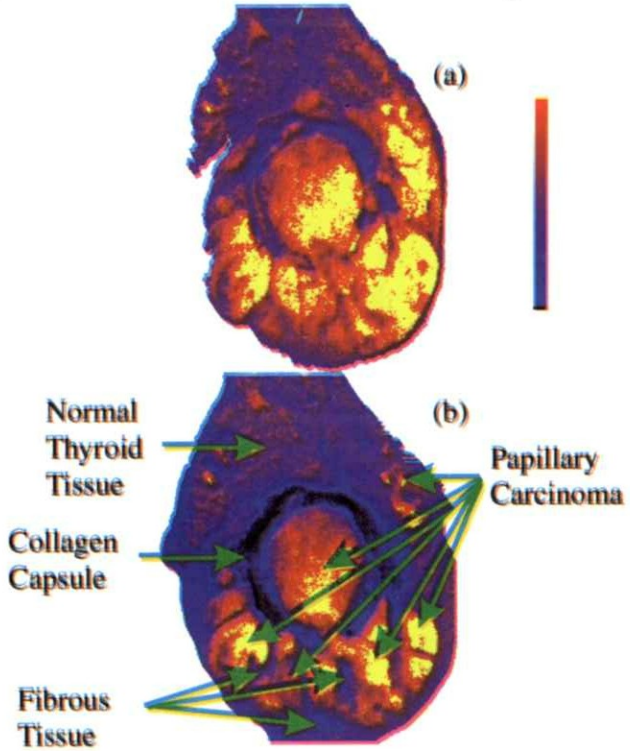

Figure 5: Papillary carcinoma thyroid specimen ratio maps, (a) R_1 and, (b) R_3, converted to pseudo color. Regions of tumor, normal tissue and collagen capsule marked in (b) were determined by histopathology.

Fig 2(b) (λ_{ex} = 300 nm; λ_{em} = 380 nm) exhibits similar features as the image seen in Fig. 2(a), but with less intensity since this filter combination primarily images the long wavelength tail of the tryptophan emission. In Figs. 2(c) (λ_{ex} = 300 nm; λ_{em} = 440 nm), 2(d) (λ_{ex} = 340 nm; λ_{em} = 380 nm), 2(e) (λ_{ex} = 340 nm; λ_{em} = 440 nm), and 2(f) (λ_{ex} = 380 nm; λ_{em} = 440 nm) the capsule, with its high collagen content, has considerably higher emission than the surrounding tissue. In particular, the image shown in Fig. 2(e) with the excitation and emission wavelengths closest to collagen absorp-

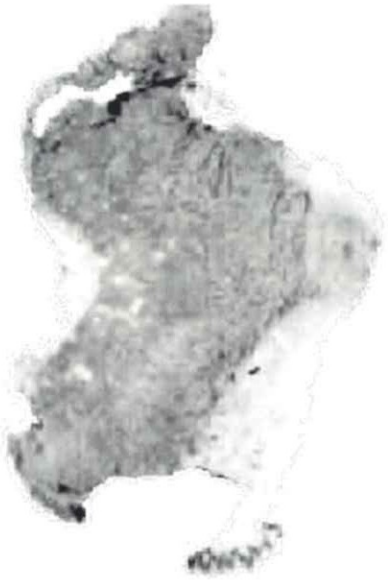

Figure 6: Histology photomicrograph of well differentiated squamous cell carcinoma on a base of tongue specimen.

tion and emission bands maxima, respectively, exhibited very high emission from the capsule, and very weak emission from the tumor within and below the capsule. The dark area on the bottom of the ring corresponds to the break where the tumor has broken out of the capsule. A low magnification histology photomicrograph of this specimen is presented in Fig. 3. Under higher magnification, it can be seen that, in addition to the tumor in the capsule, there are well defined areas of tumor separated by fibrous tissue at the bottom and left of the specimen.

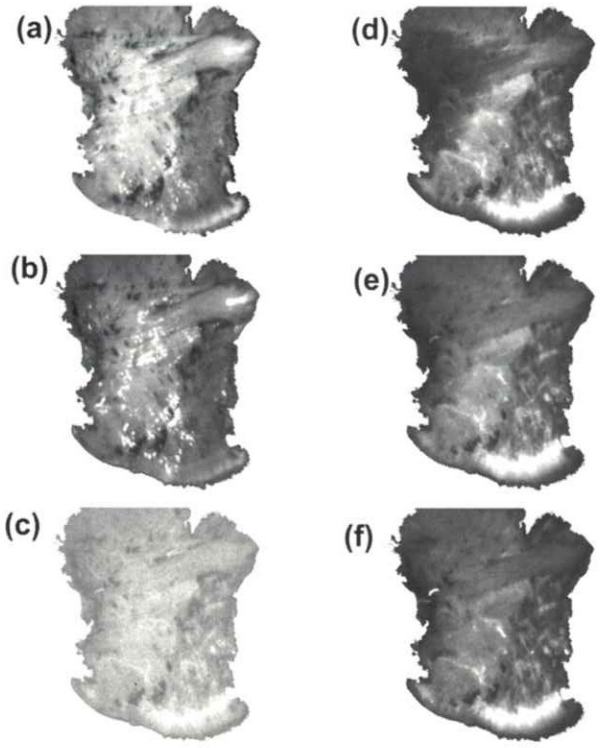

Figure 7: Fluorescence images from the base of tongue squamous cell carcinoma shown in Fig. 6. Excitation/emission wavelengths are: (a) λ_{ex} = 300 nm, λ_{em} = 340 nm; (b) λ_{ex} = 300 nm, λ_{em} = 380 nm; (c) λ_{ex} = 300 nm, λ_{em} = 440 nm; (d) λ_{ex} = 340 nm, λ_{em} = 380 nm; (e) λ_{ex} = 340 nm, λ_{em} = 440 nm; and (f) λ_{ex} = 380 nm, λ_{em} = 440 nm. The tumor covers most of the left side of the specimen.

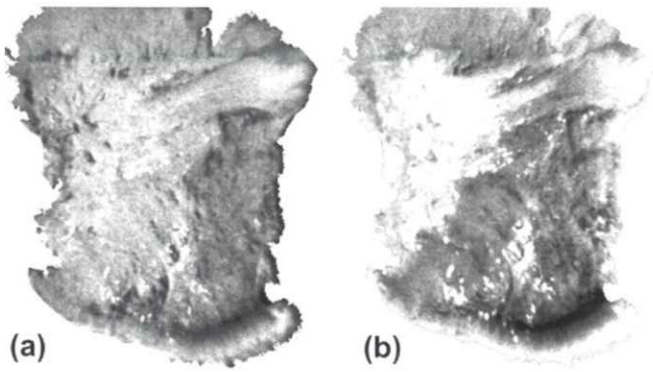

Figure 8: Intensity ratio maps generated from the fluorescence images shown in Figure 7. Ratio wavelengths are: (a) R_1 (I_{340}/I_{440}, λ_{ex} = 300 nm) and (b) R_3 (I_{300}/I_{340}, λ_{em} = 380 nm).

The contrast between the normal and cancer regions may be increased by the generation of intensity ratio maps from the fluorescence images. This was investigated by generating four ratio maps (see Table I) from this specimen. These maps are displayed in Figures 4(a)-(d). In all four ratio maps, the collagen capsule can be clearly identified. However, the maps generated using R_1 (I_{340}/I_{440}, λ_{ex} = 300 nm) and R_3 (I_{300}/I_{340}, λ_{em} = 380 nm), shown in Figs. 4(a) and (c), respectively, exhibited high contrast between normal and malignant regions. On the other hand, the R_2 (I_{380}/I_{440}, λ_{ex} = 340 nm) and R_4 (I_{340}/I_{380}, λ_{em} = 440 nm) ratio maps,

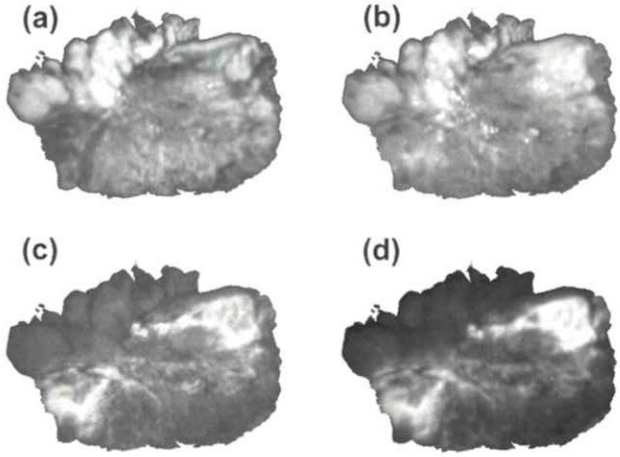

Figure 9: Fluorescence images from a moderately differentiated squamous cell carcinoma of a base of tongue specimen. The tumor is located in the upper left region of the specimen. Excitation/emission wavelengths are: (a) λ_{ex} = 300 nm, λ_{em} = 340 nm; (b) λ_{ex} = 300 nm, λ_{em} = 380 nm; (c) λ_{ex} = 300 nm, λ_{em} = 440 nm; and (d) λ_{ex} = 340 nm, λ_{em} = 380 nm.

shown in Figs. 4(b) and (d), respectively, while clearly identifying the capsule, were less effective in distinguishing the normal tissue from the malignant areas. A comparison of the R_1 and R_3 ratio maps to the histology photomicrograph demonstrated that the tumor regions can be identified in the ratio maps as areas of high ratio, i.e. low collagen emission. Regions in which the tumor has broken out of the capsule are evident in bottom part of the specimen as regions of high ratios with interspersed fibrous material appearing as dark areas (low ratio). The normal tissue regions on the top of the specimen also exhibited relatively low R_1 and R_3 ratios as compared to the tumor areas. The contrast of the ratio maps can be further enhanced by the use of pseudo color. Pseudo color maps would be particularly advantages for display on the computer monitor, and could be updated in real time. This is high contrast resulting from pseudo color is demonstrated in the color ratio maps shown in Figs 5(a) and (b) for ratio maps R_1 and R_3, respectively. In these maps, regions of high ratio (bright red to yellow) are cancer while the collagen capsule and normal tissue areas are low ratio (black to blue).

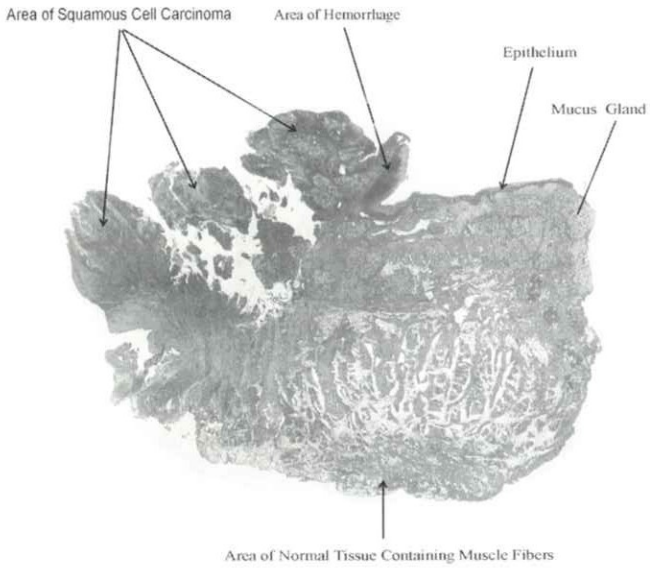

Figure 10: Histology photomicrograph of the specimen imaged in Figure 9.

Base of the Tongue Squamous Cell Carcinoma

The second specimen is a well differentiated squamous cell carcinoma of the base of tongue. A histology photomicrograph is shown in Fig. 6. The six fluorescence images acquired from the specimen are displayed in Figs 7(a)-(e), corresponding to the following excitation - emission wavelength pairs: 7(a) λ_{ex} = 300 nm, λ_{em} = 340 nm; 7(b) λ_{ex} = 300 nm, λ_{em} = 380 nm; 7(c) λ_{ex} = 300 nm, λ_{em} = 440 nm; 7(d) λ_{ex} = 340 nm, λ_{em} = 380 nm; 7(e) λ_{ex} = 340 nm, λ_{em} = 440 nm; and 7(f) λ_{ex} = 380 nm, λ_{em} = 440 nm. This specimen has areas of tumor covering most of the left side of the specimen. The tumor region appears in the images shown in Figs. 7(a) and (b) as a region of high emission intensity. i.e. high tryptophan emission. Across the middle of the sample is muscle tissue which can be seen in both Figs. 7(a) and (b). Blood vessels are located both in the far left of the sample and on the right side of the specimen. Blood vessels, due to the high absorption of hemoglobin exhibit almost no fluorescence. Epithelium can be seen at the bottom of the specimen, identifiable by its high emission intensity at 380 and 440 nm, as seen in Figs. 7(c),(d),(e) and (f). The R_1 (I_{340}/I_{440}, λ_{ex} = 300 nm) and R_3 (I_{300}/I_{340}, λ_{em} = 380 nm) ratio maps generated for this sample demonstrated high contrast between the tumor and normal regions of tissue. These ratio maps are shown in Figs. 8(a) and (b), respectively.

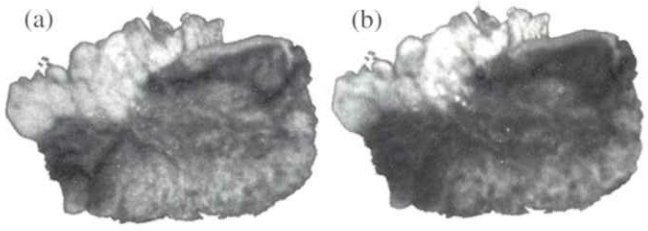

Figure 11: Intensity ratio maps generated from the fluorescence images shown in Figure 9. Ratio wavelengths are: (a) R_1 (I_{340}/I_{440}, λ_{ex} = 300 nm) and (b) R_3 (I_{300}/I_{340}, λ_{em} = 380 nm).

The third sample presented in this paper is a moderately differentiated squamous cell carcinoma, also of the base of tongue. This tissue has areas of tumor in upper left portion, mucus glands in the upper right portion, epithelium along the upper right edge, and muscle and fat in the lower part of the specimen. Four fluorescence images were acquired from this specimen and are displayed in Figs. 9(a)-(d), corresponding to the following excitation - emission wavelength combinations: 9(a) λ_{ex} = 300 nm, λ_{em} = 340 nm; 9(b) λ_{ex} = 300 nm, λ_{em} = 380 nm; 9(c) λ_{ex} = 300 nm, λ_{em} = 440 nm; and 9(d) λ_{ex} = 340 nm, λ_{em} = 380 nm. The tumor area is evidenced by a high tryptophan emission at 340 and 380 nm, Figs 9(a) and (b), respectively. This same region exhibits very weak fluorescence at 440 nm and 380 nm (λ_{ex} = 340 nm) due to the lack of collagen in the tumor. The mucus glands exhibit strong emission at 380 and 440 nm. Their location can be identified by the high intensity region at the upper right of the specimen. Additional mucus glands are located in the bottom left of the specimen. Their emission can be observed in Figs. 9(c) and (d). The lower half of the specimen consists of regions of fat and muscle. The fatty regions do not exhibit strong emission at 380 and 440 nm, since fat emits at shorter wavelengths (13,14). Muscle, having low collagen content, does not exhibit strong emission at 380 nm. A histology photomicrograph of this specimen is shown in Fig. 10. From the fluorescence images, the R_1 and R_3 ratio maps were found to show high contrast between the normal and tumor areas. These maps are presented in Figs. 11(a) and (b). In

both maps, the tumor region exhibits a high ratio while the normal regions, including the areas of fat, mucus glands, and muscle all exhibit a low ratio, demonstrating the effectiveness of these ratio algorithms.

Conclusion

This work demonstrates that fluorescence imaging of head and neck tissues can identify regions of tumor and other tissue structures. Optical Biopsy imaging can be applied in a clinical setting for the detection or cancer and precancer, or to define the margins of a tumor, noninvasively and without undo interference to current clinical examination procedures. This imaging technology will increase the effectiveness of spectroscopic examination of tissue by increasing the size of tissue regions that can be interrogated. High spatial resolution may allow detection of small foci of malignant cells, thus increasing the likelihood of early detection.

Acknowledgments

This work has been supported by grants from New York State Office of Science, Technology and Academic Research (NYSTAR) and the NASA IRA program. We thank Mediscience Technology Corp for use of their instrument to carry out this study.

References and Footnotes

1. Alfano, R. R., Tang, G., Pradham, A., Lam, W., Choy, D. S. J., and E. Opher Fluorescence spectra from cancerous and normal human breast and lung tissues, *IEEE Journal of Quantum Electronics. QE-23,* 1806, (1987).
2. Alfano, R. R., Tata, D., Cordero, J., Tomashefsky, P., Longo, F. W., and Alfano, M. A. Laser induced fluorescence spectroscopy from native cancerous and normal tissues, *IEEE J Quantum Electron. 20,* 1507, (1984).
3. Das, B. B., Glassman, W. L., Alfano, R. R., Cleary, J., Prudente, R., Celmer, E and Lubicz S. UV-fluorescence spectroscopic technique in the diagnosis of breast, ovarian, uterus, and cervix cancer. In: Laser-Tissue Interaction II, Vol. *1427,* SPIE Proceedings, Los Angeles, CA, 368, (1991).
4. Alfano, R. R., Das, B. B., Cleary, J., Prudente, R., and Celmer E. J. Light sheds light on cancer—distinguishing malignant tumors from benign tissues and tumors, *Bull N Y Acad Med. 67,* 143, (1991).
5. Glassman, W. S., Liu, C. H., Tang, G. C., Lubicz, S., and Alfano R. R. Ultraviolet excited fluorescence spectra from non-malignant and malignant tissues of the gynecological tract, *Lasers in the Life Sciences. 5,* 49, (1992).
6. Glasgold, R., Glasgold, M., Savage, H., Pinto, J., Alfano, R., and Schantz, S. Tissue autofluorescence as an intermediate endpoint in *NMBA-induced esophageal carcinogenesis, Cancer Letters. 82,* 33, (1994).
7. Ingrams, D. R., Dhingra, J. K., Roy, K., Perrault, Jr., D. F., Bottrill, I. D., Kabani, S., Rebeiz, E. E., Pankratov, M. M., Shapshay, S. M., Manoharan, R., Itzkan, I., and Feld, M. S. Autofluorescence characteristics of oral mucosa, *Head Neck. 19,* 27, (1997).
8. Dhingra, J. K., Zhang, X., McMillan, K., Kabani, S., Manoharan, R., Itzkan, I., Feld, M. S., and Shapshay, S. M. Diagnosis of head and neck precancerous lesions in an animal model using fluorescence spectroscopy, *Laryngoscope. 108,* 471, (1998).
9. Schantz, S. P., Kolli, V., Savage, H. E., Yu, G., Shah, J. P., Harris, D., Katz, A., Alfano, R. R., and H. A. G. In Vivo Native Cellular Fluorescence and Histological Characteristics of Head and Neck Cancer, *Clinical Cancer Research 4,* 1177, (1998).
10. Kolli, V. K., Savage, H. E., and Schantz, S. P. In vivo tissue autofluorescence of neoplastic aerodigestive tract mucosa, *Head and Neck. 16,* 488, (1994).
11. Kolli, V. R., Savage, H. E., Yao, T. J., and Schantz, S. P. Native cellular fluorescence of neoplastic upper aerodigestive mucosa. *Archives of Otolaryngology Head and Neck Surgery,* (1996).
12. Threshold Limit Values for Chemical Substances and Physical Agents and Biological Exposure Indices. 114. Cincinnati, OH: American Conference of Governmental and Industrial Hygienists, (1994).
13. Yang, Y., Katz, A., Celmer, E. J., Zurawska-Szczepaniak, M., and Alfano, R. R. Optical spectroscopy of benign and malignant breast tissues. *Lasers in the Life Sciences. 7,*115, (1996).
14. Katz, A., Yang, Y., Celmer, E. J., Zurawska-Szczepaniak, M., and Alfano, R. R. Fourier Diagnostic Analysis of Fluorescence Spectra from Normal and Malignant Breast Tissues. In*: OSA TOPS on Biomedical Optical Spectroscopy and Diagnostics*, Vol. *3*, Orlando, Florida, 136, (1996).

Date Received: October 26, 2001